Tunable optical filter using second-order micro-ring resonator*

Lin Deng(邓林), Dezhao Li(李德钊), Zilong Liu(刘子龙), Yinghao Meng(孟英昊), Xiaonan Guo(郭小男), and Yonghui Tian(田永辉)†

Institute of Microelectronics and Key Laboratory for Magnetism and Magnetic Materials of the Ministry of Education, School of Physical Science and Technology, Lanzhou University, Lanzhou 730000, China

(Received 17 June 2016; revised manuscript received 9 October 2016; published online 20 December 2016)

In this paper, we design and fabricate a silicon integrated optical filter consisting of two cascaded micro-ring resonators and two straight waveguides. Two micro-heaters are fabricated on the top of two micro-rings respectively, which are employed to modulate the micro-rings to perform the function of a tunable optical filter by the thermo–optic effect. The static response test indicates that the extinction ratio and 3-dB bandwidth are 29.01 dB and 0.21 nm respectively, the dynamic response test indicates that the 10%–90% rise and 90%–10% fall time of the filter are 16 μs and 12 μs, respectively, which can meet the requirements of optical communication and information processing. Finally, the power consumption of the device is also characterized, and the total power consumption is about 9.43 mW/nm, which has been improved efficiently.

Keywords: integrated optics, wavelength filtering devices, resonators, photonic integrated circuits

PACS: 42.79.Ci, 42.82.–m, 42.60.Da **DOI:** 10.1088/1674-1056/26/2/024209

1. Introduction

Tunable band-pass filters, which can be used to choose a signal with arbitrary wavelength according to the practical requirement, have important applications in optical communication and information processing.[1–4] Therefore, the tunable band-pass filter is a key research topic in the field of optical information processing. Various optical filters have been reported, including the Mach–Zehnder interferometer,[5,6] Bragg grating,[7,8] micro-ring resonator,[9–16] micro-disk resonator,[17] etc.

The micro-ring resonator (MRR) is a key building block for on-chip integrated optical information processing due to its natural features such as compact dimension, low power consumption, large-scale integration, etc. MRR has good filtering performance, resulting in popular application in WDM systems. MRR-based filters can choose the light at particular wavelengths and allow light at other wavelengths to pass through without being affected;[18–21] furthermore, compared to single MRR filters, there is a flat top spectrum performance and the out-of-band signal rejection ratio is higher for high-order MRR filters, which is very fitting for optical information processing.[22–26] The drop port of the second-order MRR is in the same direction as the input port, which is beneficial for optical network decreasing crossing in the construction. In addition, a second-order MRR structure is easier to fabricate than other higher-order MRR filters. Based on the reasons above, the second-order MRR structure has promising potential for practical application and has attracted wide attention.[27–31] Considering the outstanding performance of filtering and easy implementation in technology of the second-order MRR structure, we design and fabricate a tunable second-order MRR filter with the micro-heaters fabricated on the top of MRRs; the filtering wavelength can be exactly controlled by the voltage applied to MRRs. Compared with previous works, this device possess lower power consumption,[32] and the flexibility of this device is promoted due to the tunable filtering wavelength based on the thermo–optical effect.

2. Architecture and principle

The structure of the second-order MRR filter consisting of two cascaded MRRs and two straight waveguides is shown in Fig. 1.

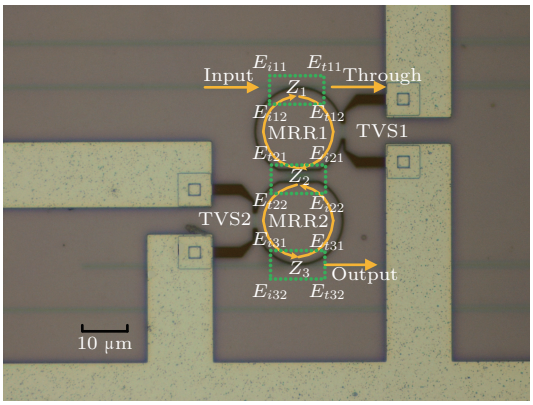


Fig. 1. (color online) Structure of high-order micro-ring resonator filter (TVS: tunable voltage source).

Continuous optical signals propagated in the upper straight waveguide can couple into MRR1 by evanescent field, and then couple into MRR2 in the same way. Finally, the

*Project supported by the National Natural Science Foundation of China (Grant No. 61405082) and the Fundamental Research Funds for the Central Universities.
†Corresponding author. E-mail: tianyh@lzu.edu.cn
© 2017 Chinese Physical Society and IOP Publishing Ltd

optical signal at the resonant wavelength can be directed to the Output port. All other optical signals at the non-resonant wavelengths will be directed to the Through port. In addition, the resonant wavelength of the second-order MRR filter can be tuned by the silicon thermo–optic effect. Therefore, the proposed device can perform the filtering performance of the filter with tunable filtering wavelength.

The performance of the second-order filter can be simulated by the scattering matrix method.[33–37] The structure of the device can be divided into three coupling regions, which is shown in Fig. 1. Each coupling region can be described by a unique scattering matrix. The scattering matrix of Z_1 can be expressed in the following form

$$\begin{bmatrix} E_{t11} \\ E_{t12} \end{bmatrix} = \begin{bmatrix} t_1 & k_1 \\ -k_1^* & t_1^* \end{bmatrix} \begin{bmatrix} E_{i11} \\ E_{i12} \end{bmatrix}, \tag{1}$$

where k_1 and t_1 are the cross-coupling coefficient and the self-coupling coefficient of the optical field amplitude, whose value depends on the specific coupling gap. The matrix is symmetric because the networks under consideration are reciprocal. Therefore, $t_1^2 + k_1^2 = 1$. Each coupling region has its unique cross-coupling coefficient when taking the maximally flat effect into consideration[38]

$$k_2^2 = 0.25k_1^4 = 0.25k_3^4, \tag{2}$$

where k_1, k_2, and k_3 are the cross-coupling coefficient of Z_1, Z_2, and Z_3, respectively. Defining a vector with the different field components P_n as follows:

$$P_n = \begin{pmatrix} -\dfrac{t_n}{k_n} & \dfrac{1}{k_n} \\ -\dfrac{1}{k_n} & \dfrac{t_{1n}^*}{k_n} \end{pmatrix}. \tag{3}$$

Equation (1) can be rewritten as

$$\begin{pmatrix} E_{i12} \\ E_{t12} \end{pmatrix} = P_1 \begin{pmatrix} E_{i11} \\ E_{t11} \end{pmatrix}. \tag{4}$$

As the optical signals propagate in the ring waveguide, it accumulates a phase shift and may be attenuated, so

$$\begin{aligned} E_{i21} &= \alpha \mathrm{e}^{\mathrm{i}\theta} E_{t12}, \\ E_{i12} &= \alpha \mathrm{e}^{\mathrm{i}\theta} E_{t21}, \end{aligned} \tag{5}$$

where α and θ are the half round trip loss and phase in both MRRs. Equation (5) can be rewritten as

$$\begin{pmatrix} E_{i21} \\ E_{t21} \end{pmatrix} = \begin{pmatrix} 0 & \alpha \mathrm{e}^{\mathrm{i}\theta} \\ \alpha^{-1} \mathrm{e}^{-\mathrm{i}\theta} & 0 \end{pmatrix} \begin{pmatrix} E_{i12} \\ E_{t12} \end{pmatrix}. \tag{6}$$

Defining a vector matrix Q as follows:

$$Q = \begin{pmatrix} 0 & \alpha \mathrm{e}^{\mathrm{i}\theta} \\ \alpha^{-1} \mathrm{e}^{-\mathrm{i}\theta} & 0 \end{pmatrix}. \tag{7}$$

The relationship between input and output described by matrix P_n and Q is

$$\begin{pmatrix} E_{i32} \\ E_{t32} \end{pmatrix} = P_1 Q P_2 Q P_1 \begin{pmatrix} E_{i11} \\ E_{t11} \end{pmatrix} = \begin{pmatrix} A & B \\ C & D \end{pmatrix} \begin{pmatrix} E_{i11} \\ E_{t11} \end{pmatrix}. \tag{8}$$

The optical power at the Drop port and the Through port of the second-order MRR filter are described as follows:

$$\begin{aligned} E_{t11} &= -\frac{A}{B} E_{i11} + \frac{1}{B} E_{i32}, \\ E_{t32} &= \frac{BC - AD}{B} E_{i11} + \frac{D}{B} E_{i32}. \end{aligned} \tag{9}$$

The matrices P_n and Q are completely general, which can account for the transfer characteristic for any frequency depending on the effective index, loss, and transmission and coupling coefficients. Furthermore, we can calculate any-order cascaded MRRs array by matrices cascading.

3. Device fabrication

The device is fabricated on an eight-inch (the unit 1 inch = 2.54 cm) silicon-on-insulator wafer with a 220-nm-thick top silicon layer and a 2 μm-thick buried SiO_2 layer. The rib waveguide with 400 nm in width, 220 nm in height, and 70 nm in slab thickness is employed to construct the device. Both MRRs have the same radii as 10 μm. Gaps between the ring waveguides and the straight waveguides are 300 nm and the gap between two micro-ring waveguides is 575 nm. After the waveguides are fabricated, 1.5 μm-thick SiO_2 is deposited on the top of the waveguides as a separate layer, and then two TiN micro-heaters with the width of 1 μm and the thickness of 120 nm are fabricated on the top of the ring waveguides. Aluminum pads with 100 μm×100 μm size are deposited to connect to the TiN micro-heaters by aluminum wires. Spot size converters (SSC) are integrated on the input and output terminals of the waveguides to enhance the coupling between the waveguides and the fibers. The SSC is a 200 μm-long linearly inversed taper with a 180-nm-wide tip.

4. Experimental results

Experimental tests of the device include a static response test, tunable performance test and dynamic response test.

4.1. Static response test

Experimental setup for the static response spectrum of the device is shown in Fig. 2. An amplified spontaneous emission source (ASE), two tunable voltage sources (TVS), and an optical spectral analyzer (OSA) are employed to characterize the static response of the device. A continuous optical wave is launched from the ASE and coupled into the input port of the device through a lensed taper fiber; two tunable voltage sources are applied to the two micro-heaters to modulate micro-rings in order to demonstrate the tunable function of the filter.

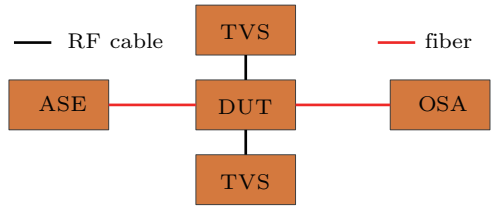


Fig. 2. (color online) Experimental setup for the static response test of the device. ASE: amplified spontaneous emission source. TVS: tunable voltage source. OSA: optical spectral analyzer. DUT: Device under test.

The measured static response spectrum of the device is shown in Fig. 3, from which we can see the extinction ratio is about 29.01 dB, the Q-factor is about 3×10^3, the free spectrum range (FSR) is about 9.52 nm, and the 3-dB bandwidth is about 0.21 nm. There are some ripples at the bottom of the spectrum, which are mainly induced by the reflections of the input and output terminals. However, these ripples do not hinder the filtering function of the device since the rolling power is too low to trigger a response.

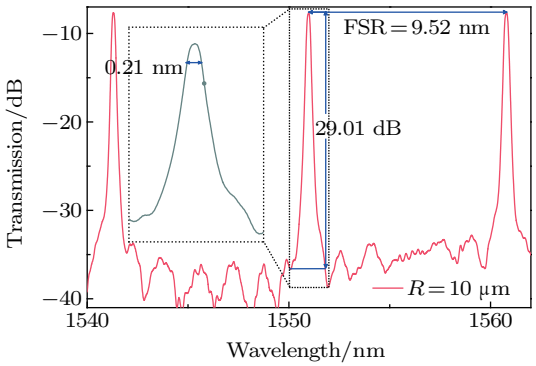


Fig. 3. (color online) Static response result of the second-order MRR filter.

4.2. Tunable performance

In order to demonstrate the tunable feature of the device, we tune the filtering wavelength with a wavelength spacing of 0.5 nm through the voltages applied to the micro-heaters by the silicon thermo–optic effect (Fig. 4).[39,40]

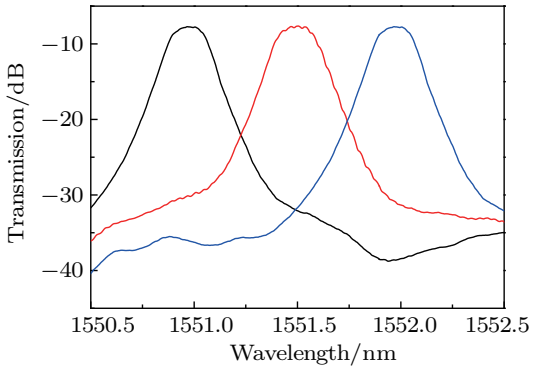


Fig. 4. (color online) Response spectra of the device with the wavelength spacing of 0.5 nm.

From Fig. 4 we can see that the filtering wavelength of the device can be continuously tuned by the applied voltages, which means the device can achieve the tunable function. The wavelength tuning range of an FSR is tested.

The power consumption performance of the device is also analyzed by tuning the filtering wavelength, which is shown in Fig. 5. Benefiting from a precise fabrication process, the two MRRs have the same resonant wavelength in the initial state, and the two micro-heaters are exactly the same. Therefore, the power consumption performances of the two MRRs are almost identical. In order to describe this simpler, we only analyze the power consumption of MRR1 in Fig. 5. It needs a threshold voltage to activate MRR1, therefore, the start point of applied voltage in Fig. 5 is not from the origin but 0.69 V, which means the threshold voltage of MRR1 is about 0.69 V. The blue dot line in Fig. 5 represents the sum power consumption of MRR1 and MRR2. The sheet in Fig. 5 shows the parameters adopted in linear fitting of the blue dot line.

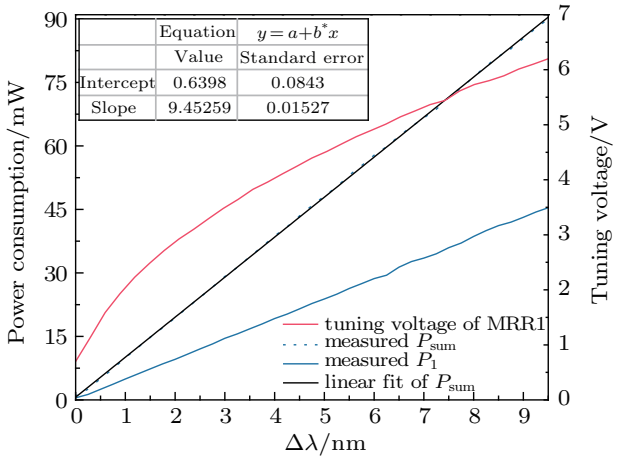


Fig. 5. (color online) Power consumption of this device. P_1 and P_2 are the power consumption of MRR1 and MRR2, respectively. P_{sum} is the sum of P_1 and P_2.

Figure 5 indicates that the device can be tuned under the total power consumption of 9.45 mW/nm linearly. Further optimization should be done to further decrease the power consumption, such as etching air trenches below the device.[41]

4.3. Dynamic response test

The dynamic response is characterized by a tunable laser, a two-channel arbitrary function generator (AFG), a photodiode detector and an oscilloscope. The monochromatic light with the wavelength of 1550.98 nm output from the tunable laser is coupled into the device through a lensed fiber. Two binary sequences non-return-to-zero signals at 20 kbps generated by the two-channel AFG are applied to MRR1 and MRR2, respectively. The output light signal is transformed to an electrical signal by a photodiode detector. All the two input and output electrical signals are fed into a multi-channel oscilloscope for waveform observation.

Figure 6 indicates that the device responds well to the 20 kbps thermally tuning signal. The 10%–90% rise and 90%–10% fall time are 16.0 μs and 12.0 μs, respectively.

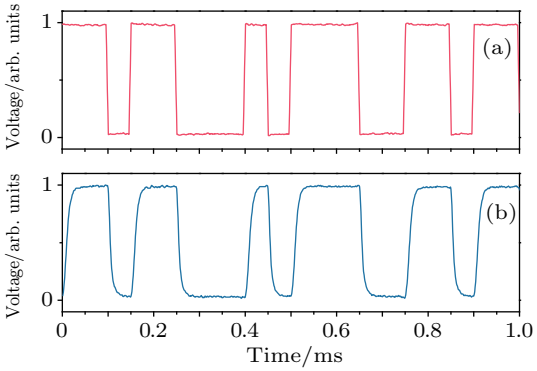


Fig. 6. (color online) Dynamic response result of the second-order MRR filter: (a) applied voltage and (b) photodiode voltage.

5. Conclusions

In order to achieve an outstanding performance in filtering and easy implementation in technology, a structure of the second-order MRR filter consisting of two cascaded MRRs and two straight waveguides was proposed. This structure has been analyzed by the scattering matrix method. In this method, each coupling region can be described by a unique scattering matrix and any-order cascaded MRRs array can be calculated by matrices cascading. In addition, we have fabricated and tested a second-order micro-ring filter in this paper, which has an extinction ratio of 29.01 dB with a 3-dB bandwidth of 0.21 nm. It can be thermally tuned over the whole FSR with the tuning efficiency of 9.45 mV/nm. The 10%–90% rise and 90%–10% fall time of the filter are 16.0 μs and 12.0 μs, respectively, which is fast enough for the applications of the tunable optical filter.

References

[1] Madsen C K and Zhao J H 1999 *Optical filter design and analysis* (New York: Wiley) pp. 7–14

[2] Reed G T and Knights A P 2004 *Silicon photonics: an introduction* (New York: Wiley) pp. 355–394

[3] Hohlfeld D, Bechtold T and Zappe H 2005 *Dimension Reduction of Large-Scale Systems* (Springer) pp. 337–340

[4] Philip J, Jaykumar T, Kalyanasundaram P and Raj B 2003 *Meas. Sci. Technol* **14** 1289

[5] Absil P P, Hryniewicz J V, Little B E, Wilson R A, Joneckis L G and Ho P T 2000 *IEEE Photon. Technol. Lett.* **12** 398

[6] Inoue K, Kominato T and Toba H 1991 *IEEE Photon. Technol. Lett.* **3** 718

[7] Hunter D B and Minasian R A 1996 *IEEE Microw. Guided Wave Lett.* **6** 103

[8] Atherton P, Reay N K, Ring J and Hicks T 1981 *Opt. Eng.* **20** 206805

[9] Dong J J, Liu L, Gao D S, Yu Y, Zheng A L, Yang T and Zhang X L 2013 *IEEE Photon. J.* **5** 5500307

[10] Chu S T, Little B E, Pan W G, Kaneko T, Sato S and Kokubun Y 1999 *IEEE Photon. Technol. Lett.* **11** 691

[11] Stamatiadis C, Vyrsokinos K, Stampoulidis L, Lazarou I, Maziotis A, Bolten J, Karl M, Wahlbrink T, Heyn P D, Sheng Z, Thourhout D V and Avramopoulos H 2011 *J. Lightw. Technol.* **29** 3054

[12] Griffel G 2000 *IEEE Photon. Technol. Lett.* **12** 810

[13] Little B E, Foresi J, Steinmeyer G, Thoen E, Chu S T, Haus H, Ippen E, Kimerling L and Greene W 1998 *IEEE Photon. Technol. Lett.* **10** 549

[14] Geng M M, Jia L X, Zhang L, Yang L, Chen P, Wang T and Liu Y L 2009 *Opt. Express* **17** 5502

[15] Ji R Q, Yang L, Zhang L, Tian Y H, Ding J F, Chen H T, Lu Y Y, Zhou P and Zhu W W 2011 *Opt. Express* **19** 20258

[16] Ji R Q, Yang L, Zhang L, Tian Y H, Ding J F, Chen H T, Lu Y Y, Zhou P and Zhu W W 2011 *Opt. Express* **19** 18945

[17] Huang Q Z, Zhang X L, Xia J S and Yu J Z 2011 *Opt. Lett.* **36** 4494

[18] Chraplyvy A R and Tkach R W 1986 *Electron Lett.* **22** 1084

[19] Mukherjee B 2006 *Optical WDM networks* (New York: Springer) pp. 43–130

[20] Sadot D and Boimovich E 1998 *IEEE Commun.* **36** 50

[21] Xiao S, Khan M H, Shen H and Qi M 2007 *Opt. Express* **15** 7489

[22] Hryniewicz J V, Absil P P, Little B E, Wilson R A and Ho P T 2000 *IEEE Photon. Technol. Lett.* **12** 320

[23] Van V, Little B E, Chu S T and Hryniewicz J V 2004 *IEEE Leos Ann. Mtg.* **2** 571

[24] Popovic M A, Barwicz T, Watts M R, Rakich P T, Socci L, Ippen E P, Kartner F X and Smith H I 2006 *Opt. Lett.* **31** 2571

[25] Xia F N, Rooks M, Sekaric L and Vlasov Y 2007 *Opt. Express* **15** 11934

[26] Little B E, Chu S T, Absil P P, Hryniewicz J V, Johnson F G, Seiferth E, Gill D, Van V, King O and Trakalo M 2004 *IEEE Photon. Technol. Lett.* **16** 2263

[27] Zhu X L, Li Q, Chan J, Ahsan A, Lira H L R, Lipson M and Bergman K 2012 *IEEE Photon. Technol. Lett.* **24** 1555

[28] Liu L, Yang T, Dong J J 2014 *Chin. Phys. B* **23** 093201

[29] Xiong K, Xiao X, Hu Y T, *et al.* 2012 *Chin. Phys. B* **21** 074203

[30] Xu Q, Schmidt B, Shakya J and Lipson M 2006 *Opt. Express* **14** 9431

[31] Chu S T, Little B E, Pan W G, Kaneko T and Kokubun Y 1999 *IEEE Photon. Technol. Lett.* **11** 1426

[32] Hu T, Wang W J, Qiu C, Yu P, Qiu H Y, Zhao Y, Jiang X Q and Yang J Y 2012 *IEEE Photon. Technol. Lett.* **24** 524

[33] Amiri I S and Afroozeh A 2015 *Advances in Laser and Optics Research* (New York: Nova Science)

[34] Yariv A, Xu Y, Lee R K and A Scherer 1999 *Opt. Lett.* **24** 711

[35] Yariv A 2002 *IEEE Photon. Technol. Lett.* **14** 483

[36] Poon J K S, Scheuer J, Mookherjea S, Paloczi G T, Huang Y Y and Yariv A 2004 *Opt. Express* **12** 90

[37] Schwelb O 2004 *J. Lightw. Technol.* **22** 1380

[38] Little B E, Chu S T, Haus H A, Foresi J and Laine J P 1997 *J. Lightw. Technol.* **15** 998

[39] Kiyat I, Aydinli A and Dagli N 2006 *IEEE Photon. Technol. Lett.* **18** 364

[40] Cocorullo G, Della F G, Rendina I and Sarro P M 1998 *Sens. Actuators A-Phys.* **71** 19

[41] Dong P, Qian W, Liang H, Shafiiha R, Feng D Z, Li G L, Cunningham J E, Krishnamoorthy A V and Asghari M 2010 *Opt. Express* **18** 20298